

Failure Investigation of Boiler Tubes Failed Due to Thermal Fatigue and Corrosion Fatigue

Aditya Gokhale, Deepak Kumar Gope, Prahlad Halder, Anil Kumar Das, Anand D Varma*

Advanced Materials Research Lab, NTPC Energy Technology Research Alliance, NTPC Ltd.,
Greater Noida, Uttar Pradesh, India.
anandvarma@ntpc.co.in

Abstract. Flexible operations cause base load fluctuations in the power demand affecting the boiler operation. Failure due to thermal fatigue occurs for components subjected to cyclic load fluctuations. These fluctuations can be of mechanical or thermal nature. Corrosion fatigue is a special case of thermal fatigue wherein the damage is accentuated because of the action of corrosion occurring on the internal surface of the tube. In the present failure investigation, three different tubes were investigated viz., two water wall tubes and one economizer tube. The water wall tubes failed due to thermal fatigue, despite experiencing corrosive environment. Whereas, the economizer tube experienced corrosion fatigue environment. The investigation also points out that although, corrosion fatigue is a sub-set of thermal fatigue, it is necessarily not true that the tube should also experience overheating conditions.

Keywords: Thermal fatigue, corrosion fatigue, Ferrite, Pearlite.

1. Introduction

The coal fired power plant is the main backbone of India's power sector with an estimated share of close to 71% [1]. However, with recent emission norms and climatic challenges the renewable sector needs a big and immediate boost. The phasing out of old power plants, erratic supply nature of renewable power and the necessity to sustain the grid requirements puts pressure on all the available sources of power generation. Factors like wind, sunlight and climatic changes can cause erratic and unpredictable power generation from the renewables; this calls for flexible operation of power plants. The coal-fired boilers were designed for base-load operation with an operational timeline of close to 25 years. This results in selecting boiler materials which have better high-temperature creep performance capable of withstanding temperatures for longer time. However, flexible operation leads to thermal load fluctuations in boiler, which calls for materials that can withstand fluctuating loads and different temperatures. Although, fatigue and creep are design considerations, but these factors are considered

for base load, general loads and unsteady temperature and pressure changes, boiler shutdowns and start-ups. However, due to the flexible operations, fatigue failure is also, now, becoming a harsh reality.

Boiler water walls are generally composed of SA-210 GrA/C and SA-213 T-22 grade materials [2,3]. These materials have high creep strength and high corrosion resistance. During operation the boiler is hot with the metal temperatures going as high as 700°C near the metal surface. Failure analysis by some authors have shown fatigue to be the primary cause. Failure analysis by Ahmad et.al.,[4] of a SA-210 A1 grade material showed that the wall side tubes failed due to a combination of thermal fatigue, corrosion fatigue and creep damage. Arora et.al., [5] investigated fatigue in carbon steel tubes under multiaxial loading. Azevedo et.al.,[6] investigated failure in a heat exchanger serpentine belonging to a vertical heat exchanger. The steel serpentine was made up of ASTM A 178 Grade A. The material failed just 2 years in service and the microstructure analysis showed wedge type cracks and de-carburization. Himarosa et.al., [7] conducted failure root cause analysis on platen-superheater and water confirmed that the crack propagation was under the influence of cyclic loading. Smith et.al., [8] conducted failure analysis for 0.5Cr-0.5Mo and 2.25Cr-1Mo boiler tubes. Circumferentially aligned cracks were observed which initiated due sulfidation/thermal fatigue interactions. Crack tip corrosion assists crack growth.

Secondary reasons like stress concentration, incorrect material application and prior defects can also accelerate fatigue failure. Ghosh et.al., [9] investigated failure in a boiler water wall. It was found that unstable fluid flow in the water wall can lead to vibrational fatigue due to hammering effect. These fluctuations in load coupled be already present welding defect can cause fatigue failure.

The present manuscript investigates the failures in water wall and economiser tubes composed of SA210-GrA/C and SA213 T-22 grade of material. The SA210-GrA/C tube material was obtained from a 200 MW and 500 MW power plant and SA213 T-22 tube material was obtained from a 800 MW power plant. The investigation aims to bring out the various fatigue and corrosion fatigue damage mechanisms which caused failure.

2. Methodology

2.1 Chemical composition

Chemical composition was determined using an Optical Emission Spectrometer. An average of 5 sparks per sample is presented in Table 1.

2.2 Microstructural characterization

The failed tubes were first visually examined and then appropriate regions were selected for sectioning. Other regions of interest were also selected. Sectioned tube samples were mounted using a Buehler hot press mount with Bakelite moulding. This

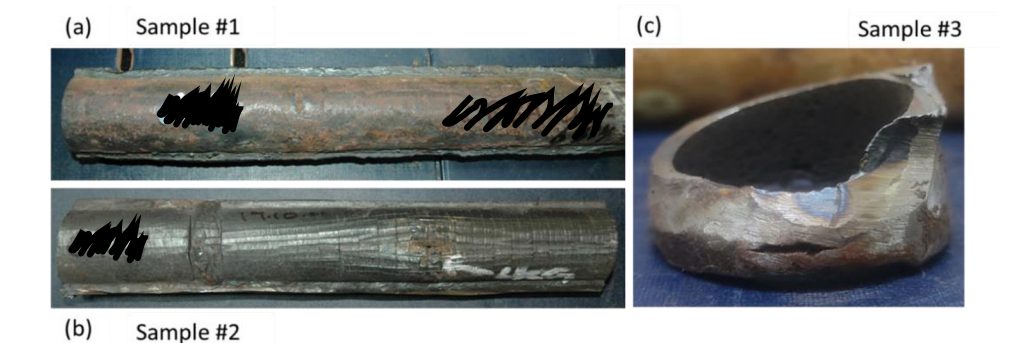


Fig. 1. Photograph of the as received failed tubes. (a) – (b) Water Wall tube (c) The stub of economiser tube connecting the header. Note: This belongs to the stub hence cutting was difficult.

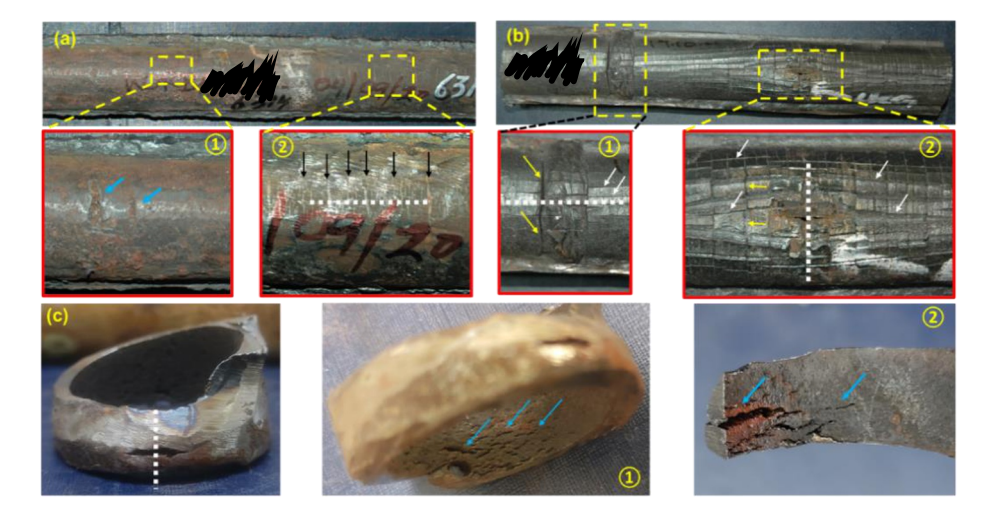


Fig. 2. Photographs of the as received failed tube showing different macro features (a) Sample#1: Water wall showing circumferentially aligned micro cracks, indicated by black arrows (b) Sample#2: Water Wall tube showing circumferentially longitudinally aligned cracks, indicated by yellow arrows and white arrows respectively. (c) Sample #3: The stub of economiser tube connecting the header. Internal surface showing numerous fissures, indicated by blue arrows. The white dotted line shows the sectioning plane for metallographic examination.

was followed by polishing on a diamond disc and SiC paper. Cloth polishing using 9 μ m and 3 μ m diamond slurries were employed. De-ionized water (DI) was used as a coolant and lubricant. A final polishing step using colloidal silica (particle size 0.01 μ m) was employed to obtain a mirror finish. The mounted samples were cleaned in an ultrasonic cleaner with ethanol as cleaning medium. The samples were rinsed with

ethanol. The microstructure before and after etching was obtained using Leica DMi8 inverted microscope. To reveal the microconstituents, etching was performed in 2% Nital (2 ml HNO₃ in 98 ml ethanol). Hardness tests were carried using Tinius Olsen Vickers Hardness (500 gf - 12 seconds dwell time), using a diamond Vickers indenter.

2.3 Visual examination

Visual examination was carried using unaided eye. A Nikon D70S digital single – lens reflex camera was used to obtain photographs of the tubes.

3. Results

Photographs of the as received failed tubes is shown in Figure 1. The chemical composition of the three samples is presented in Table 1. Sample #1 and #2 are water wall tubes conforming to SA 210-GrA and SA 213 – T22. Sample #3 is an economiser tube conforming to SA210 – GrA. The tubes showed numerous damage features. Figure 2 shows the magnified view of the different features observed on the three samples through naked eyes. Sample #1 showed no failure however it showed a dent, shown in Figure 2 (a) ① and numerous circumferential lines or serrations, shown in Figure 2 (a) ②, on the external surface. Sample #2 showed a puncture type failure, shown in Figure 2 (b) ②. Sample #2 also showed longitudinal and circumferential cracks on the external surface. Sample #3 was the region near the stub weld and there was a problem accessing and cutting the sample for analysis; as a result, a ring was sent for analysis. Severe grinding marks can be seen in Figure 1 (c).

Metallographic examination revealed the damage mechanisms. Microstructural examination of Sample #1 showed sharp notches originating from the external surface, as shown in Figure 3. The notches had a very sharp tip with thickness ~0.04 mm. The external surface also showed de-carburization, with hardness ~147 HV0.5. Sample #2

Elements (wt. %)							
Sample	С%	Si%	Mn%	S%	P%	Cr%	Mo%
Sample #1	0.29 ± 0.003	0.27 ± 0.0025	$\begin{array}{c} 0.81 \\ \pm 0.003 \end{array}$	$\begin{array}{c} 0.024 \\ \pm \ 0.001 \end{array}$	$\begin{array}{c} 0.016 \\ \pm \ 0.001 \end{array}$	-	-
SA 210 – Gr A	0.35 Max	0.1 Min	0.29 – 1.06	0.035 Max	0.035 Max	-	-
Sample #2	$0.0816 \\ \pm 0.003$	0.19 ± 0.002	0.44 ± 0.001	$\begin{array}{c} 0.003 \\ \pm \ 0.0001 \end{array}$	$\begin{array}{c} 0.0012 \\ \pm \ 0.0001 \end{array}$	$\begin{array}{c} 2.43 \\ \pm \ 0.001 \end{array}$	$\begin{array}{c} 0.93 \\ \pm 0.002 \end{array}$
SA213 T22	0.05 - 0.15	0.5 Max	0.3 - 0.60	0.025 Max	0.025 Max	1.90 – 2.60 0.87 – 1.13	
Sample #3	$\begin{array}{c} 0.12 \\ \pm \ 0.002 \end{array}$	$\begin{array}{c} 0.20 \\ \pm \ 0.002 \end{array}$	0.55 ± 0.002	0.017 ± 0.0002	0.014 ± 0.0003	-	-
SA 210 – Gr A	0.35 Max	0.1 Min	0.29 – 1.06	0.035 Max	0.035 Max	-	-

showed both longitudinal and circumferential cracks, as seen in Figure 1 (b). Microstructural examination of Sample #2, near the puncture failed region, showed extensive thinning, as seen in Figure 4 (a). The failed edge showed numerous elongated voids (Figure 4 (b) & (c)). External surface showed marginal decarburized layer and small notches originating from the external surface. Closer examination of these notches revealed that oxidation progressed on the grain boundaries (shown in Figure 4 (f)). The microstructure showed extensive degradation with a considerable loss in the hardness wherein the hardness was $124 \pm 7 \text{ HV}0.5$. The circumferential cracks were observed originating from the external surface and travelling along the heat affected zone (HAZ) of the weld, as seen in Figure 5. Voids were also observed in the weld bead region (shown in Figure 5 ②). Hardness profile around the weld, base metal and HAZ showed a considerable drop in hardness. The hardness for this material is around 170 - 180 HV 0.5 [10]. However, in the present case the hardness has dropped to approximately 130 HV 0.5.

The economiser stub tube was received in a poor condition. The internal surface, shown in Figure 6, showed numerous fissures, indicated by magenta arrows. Some of the fissures have combined to form a large crack, indicated by red arrow. As opposed to the fatigue failure, the cracks in this sample originated from the internal surface, as shown in Figure 6 (b) - (d). Corrosion pits were evident and the corrosion also proceeded laterally (seen in Figure 6 (e)). It can be observed that the notches are originating from the internal surface and do not bear a sharp tip but rather a blunt bulbous head. This is a sign of prevailing corrosion activity. The hardness was in the range 147 - 150 HV0.5.

4. Discussion

The introduction of renewable power to tackle climate change has changed the energy production scenario. However, the dependence of renewables on sun, wind and water makes the dispatch of electricity erratic. This leads to erratic demands on coal fired power plants thereby calling a need for flexible operations which leads to erratic pressure and temperature fluctuations in the boiler [11]. A boiler is designed for baseload operations, some start-up and shut-down cycle along with special emphasis on long term properties such as creep. The effect of cyclic thermal stresses is similar to that induced by fluctuating or cyclic mechanical stresses. It may also occur in the regions where turbulent mixing of the fluids leads to rapid thermal transitions. All these factors are leading to fatigue failures in boiler tubes and headers. Besides temperatures there are other factors as well which contribute to the fatigue cracking. Some of the factors, and not limited to, are header expansion, piping loads, moment restraints and stub welds where header tubes are joined. Shibli et.al., [12] have discussed the plant and research experience in P-91 Martensitic Steel. The ability of low thickness components to reach thermal equilibrium is faster. Thus, higher strength steel grades like P-91, offers the potential to make thin-walled tubes. However, weld failures under

creep-fatigue interactions leading to Type-IV cracking was observed under simulated and service conditions. The M₂₃C₆ types of precipitates and Laves phase form faster in the fine grain HAZ region of 9Cr martensitic steels making them prone to cracking [11]. Azevedo et.al., [6] investigated the failure in an ASTM A 178 Grade A serpentine of a heat exchanger and concluded that cracking, leading to eventual failure, was due to thermal cycling. Cracks perpendicular to tube axis (i.e. transverse cracking) was observed on the external surface of the tube and same was observed in the microstructure. Figure 2 (a) and (b), shows the SA 210 - Gr.A and SA 213- T-22 water wall tubes wherein the transverse cracking is clearly evident. Microstructural examination also showed cracks originating from the external surface. Figure 3 shows the microstructure for Sample #1. It can be seen that the sharp notches originate from the external surface. Figure 3 (b) and (e) shows the sharp notches. One of the notches has almost consumed the entire thickness of the tube (Figure 3 (b)). The sharpness of the notch can be attributed to the frequency of fluctuation [13]; the higher the frequency of fluctuation the sharper the notch and a thinner base and vice-versa. The presence of de-carburization layer, shown in Figure 3 (c), is also evidence of the tube experiencing overheated conditions. Sample #2 showed a puncture type failure, transverse and longitudinal cracking, shown in Figure 2 (b). Longitudinal type cracking is a sign of short-term or long-term overheating failure; however, transverse type of cracking is a sign of thermal-fatigue failure [14]. Microstructural examination near the puncture failure showed presence of elongated creep voids; creep is a sign of long-term overheating. The presence of a decarburized layer, shown in Figure 4 (c), and the degraded microstructure, shown in Figure 4 (f), are signs of overheating. Fatigue crack propagation is from the external surface. Figure 4 (d) shows the cracking in the external surface and penetrating the tube metal. The near tip region of the crack tip, shown in Figure 4 (e), shows that the oxide filled crack propagation occurs on grain boundary (as indicated by black arrows in Figure 4 (e)). Vetriselvan et.al., [15] investigated thermal fatigue in T-91. They observed that in an unconstrained T91 tube crack initiation on the ID side of the tube was observed after 5000 cycles. Shibli et.al., [12] also pointed out, although debatable, that thicker components, under cycling duty, are more likely to fail than in base load plant.

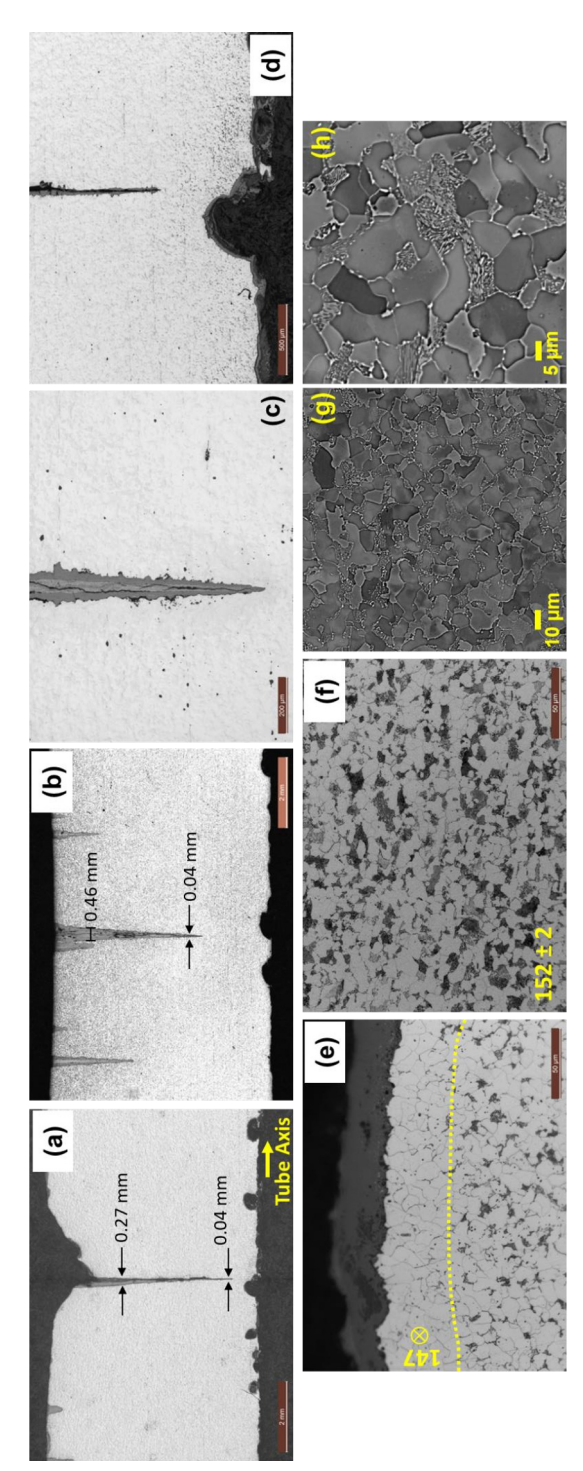


Fig. 3. Sample #1. (a) Longitudinal cross section showing the wedge type feature. (b) The wedge feature has almost consumed the entire thickness of the tube. (c) De-carburization can be observed on the external surface, demarcated by yellow dotted line. (d) Longitudinal cross section of the tube showing multiple wedge features. (e) The circumferentially aligned wedges are oxide filled with sharp tips. (f) Optical image showing the Ferrite-Pearlite microstructure. The numbers indicate the Vickers hardness at that particular location.

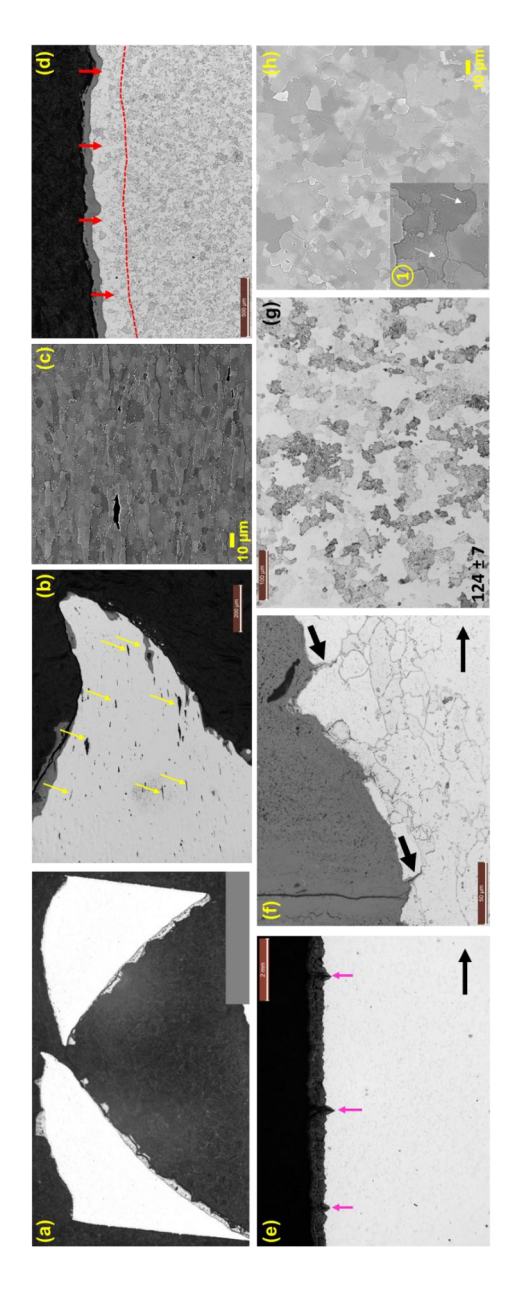


Fig. 4. Sample #2. (a) Circular cross section showing the failed edge. (b) Magnified image of the failed edge. The wedge feature has almost consumed the entire thickness of the tube. (c) De-carburization can be observed on the external surface, demarcated by yellow dotted line. (d) Longitudinal cross section of the tube showing multiple wedge features. (e) The circumferentially aligned wedges are oxide filled with sharp tips. (f) Optical image showing the Ferrite-Pearlite microstructure.

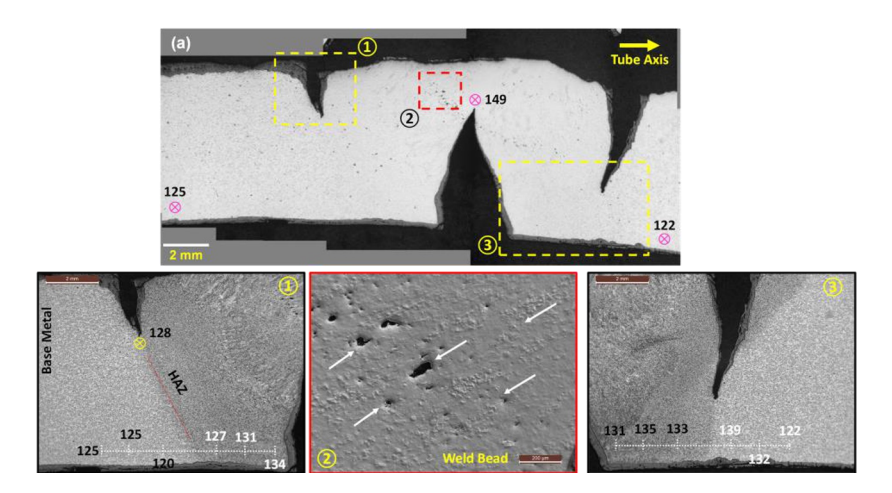


Fig. 5. Sample #2. (a) Microstructure of the welded region showing the cracks. Note that these cracks are wider than the ones observed in sample #1. (1) and (3) shows the cracks initiating from the external surface along the HAZ. (2) Shows the weld bead region with numerous creep voids in the weld bead region. The numbers indicate the hardness.

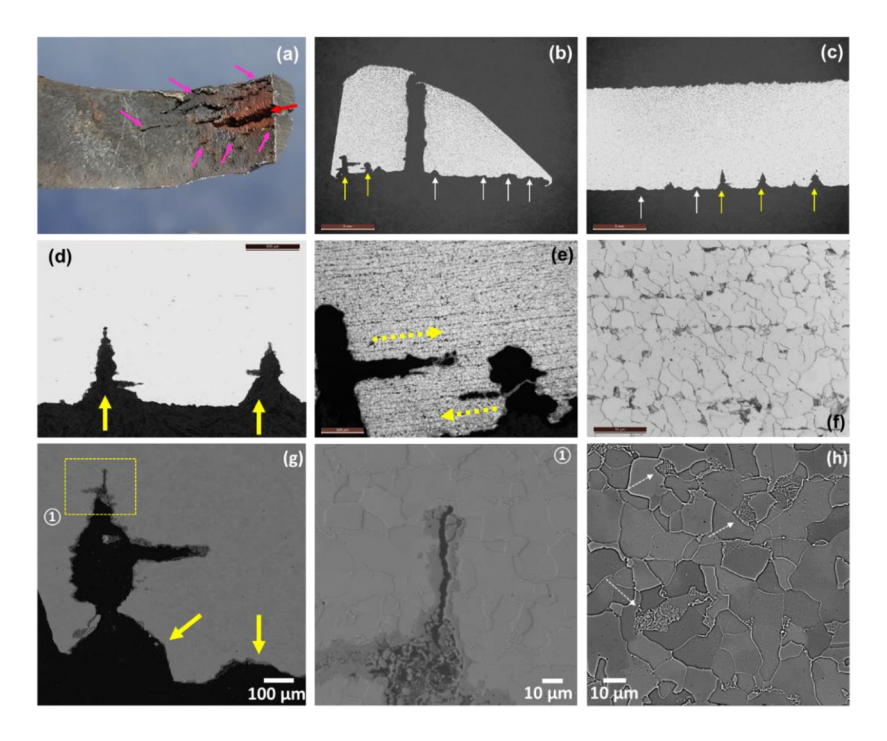


Fig. 6. Sample #3. (a) Photograph of the internal surface of the weld stub region showing numerous fissures, indicated by magenta arrows, and the large crack, indicated by red arrow. (b) – (d) Microstructure of the failed region showing the corrosion pits, indicated by white arrows, and the corrosion fatigue cracks, indicated by yellow arrows. (e) Microstructure near the corrosion fatigue crack showing the lateral corrosion attack. (d) Microstructure showing healthy Ferrite-Pearlite.

Corrosion fatigue is fatigue in corrosive environment. The fatigue cracks originate from the internal surface as pitting due to corrosion makes these site vulnerable for crack initiation. Ahmad et.al., investigated failure in SA 210-A1 grade tube. It was observed that the internal surface showed evidence of corrosion on the internal side of the tube. Transgranular cracks were found to originate from the internal surface of the tube with the origins tracing back to the base of the corrosion pit. Ahmad et.al., [16] concluded that one of the tubes failed due to corrosion fatigue and also interplay of thermal fatigue and creep-fatigue interaction. Corrosion fatigue is usually catastrophic and calls for an immediate shutdown due to failure. Generally, corrosion fatigue initiates from the internal side in water wall tubes and appears as multiple fissures on the internal side, which are visible through naked eyes; these fissures combine to form a larger crack [17][18]. In the present case the internal surface of the failed tube showed extensive fissures and cracking, shown in Figure 6 (a). Metallographic examination revealed that the internal surface showed corrosion pits, shown in Figure 6 (b) and (c). Notches originating from the internal surface were also observed, as shown in Figure 6 (d) and (e). The optical image, shown in Figure 6 (f), shows a Ferrite-Pearlite microstructure. The cracks are originating from the internal surface of the tube. Unlike the thermal fatigue cracks, as shown in Figure 3, these cracks have a wider base and circular or bulbous head unlike sharp tips of their thermal fatigue cracks counterparts. Furthermore, the evidence of corrosion is clear wherein it not only progresses inwards but also sideways (as seen in Figure 6 (e)).

5. Conclusion

The present failure investigation encompasses and brings out the differences between thermal fatigue and corrosion fatigue in boiler tubes.

- i. In thermal fatigue, the presence of sharp oxide filled notches originating from the external surface is a clear indication of the tube experiencing the thermal fatigue conditions.
- ii. Notches from internal surface are also indicators of thermal fatigue but they differ from the ones observed in corrosion fatigue.
- iii. In corrosion fatigue notches from the internal surface bear bulbous tip with no/negligible loss in tube metal hardness.
- iv. Evidence of metal loss from the internal (fluid) side along with sharp notches and combination of both is a good indicator of corrosion fatigue.
- v. Due to thermal fluctuations, there is a degradation of microstructure in the case of thermal fatigue, but in corrosion fatigue the degradation is not that evident.

Acknowledgement

The authors are thankful to Sh. Arun Sharma for assisting in sample preparation. The authors are also thankful to Sh. Shaswattam for his words of encouragement. Overall infrastructure support by NTPC Ltd., is also acknowledged.

Disclosure of Interests. The authors declare that they have no conflicts of interest to disclose regarding the research presented in this manuscript.

References

- [1] Govt. of India, Ministry of Coal, Generation of Thermal Power from Raw Coal, (n.d.).
- [2] ASTM, Standard Specification for Seamless Medium-Carbon Steel Boiler and Superheater Tubes, in: ASTM A210/A210M-19, 2019: p. 03.
- [3] ASTM, Standard Specification for Seamless Ferritic and Austenitic Alloy-Steel Boiler, Superheater, and Heat-Exchanger Tubes, in: ASTM A213/A213M-22a, 2023: pp. 15– 30.
- [4] S.R. Ahmed, L.A. Agarwal, B.S.S. Daniel, Effect of Different Post Weld Heat Treatments on the Mechanical properties of Cr-Mo Boiler Steel Welded with SMAW Process, Mater Today Proc 2 (2015) 1059–1066. https://doi.org/10.1016/j.matpr.2015.07.002.
- [5] P. Arora, S.K. Gupta, R.K. Singh, S. Sivaprasad, FATIGUE STUDIES ON CARBON STEEL TUBES UNDER MULTIAXIAL LOADING, 2015. https://www.researchgate.net/publication/281372112.
- [6] C.R.F. Azevedo, G.S. Alves, Failure analysis of a heat-exchanger serpentine, Eng Fail Anal 12 (2005) 193–200. https://doi.org/10.1016/j.engfailanal.2004.07.001.
- [7] R. Adi Himarosa, S. Dini Hariyanto, W. Hozaifa Hasan, M. Akhsin Muflikhun, Failure analysis of platen superheater tube, water wall tube, and sealpot plate: A case study from electricity power plant in indonesia, Eng Fail Anal 135 (2022). https://doi.org/10.1016/j.engfailanal.2022.106108.
- [8] B.J. Smith, A.R. Marder, A Metallurgical Mechanism for Corrosion-Fatigue (Circumferential) Crack Initiation and Propagation in Cr-Mo Boiler Tube Steels, n.d.
- [9] D. Ghosh, H. Roy, C. Subramanian, Metallurgical Failure Investigation of Premature Failed Platen Water Wall Tube in a Thermal Power Plant Boiler, Journal of Failure Analysis and Prevention 21 (2021) 733–737. https://doi.org/10.1007/s11668-021-01137-3.
- [10] A.S. for T. and Materials, A213/A213M-18: Standard Specification for Seamless Ferritic and Austenitic Alloy-Steel Boiler, Superheater, and Heat-Exchanger Tubes, ASTM International i (2018).
- [11] J. Heo, M. Park, J.M. Kim, D.W. Jang, J.H. Han, Effect of Flexible Operation on Residual Life of High-Temperature Components of Power Plants, Processes 11 (2023). https://doi.org/10.3390/pr11061679.

- [12] A. Shibli, F. Starr, Some aspects of plant and research experience in the use of new high strength martensitic steel P91, International Journal of Pressure Vessels and Piping 84 (2007) 114–122. https://doi.org/10.1016/j.ijpvp.2006.11.002.
- [13] James J Dillon, Paul B Desch, Tammy S Lai, The Nalco Guided to Boiler Failure Analysis, second edition, 2011.
- [14] J. Dillon, P. Desch, T. Lai, D. Flynn, The Nalco Guide to Boiler Failure Analysis, Second Edition, The McGraw-Hill Companies, 2011.
- [15] R. Vetriselvan, P. Sathiya, G. Ravichandran, Experimental and numerical investigation on thermal fatigue behaviour of 9Cr 1Mo steel tubes, Eng Fail Anal 84 (2018) 139–150. https://doi.org/10.1016/j.engfailanal.2017.11.005.
- [16] J. Ahmad, J. Purbolaksono, L.C. Beng, Thermal fatigue and corrosion fatigue in heat recovery area wall side tubes, Eng Fail Anal 17 (2010) 334–343. https://doi.org/10.1016/j.engfailanal.2009.06.014.
- [17] Testex, Corrosion Fatigue Cracking Paper, (n.d.).
- [18] Materials R-Tech, EpicFail Corrosion Fatigue, (n.d.).

Open Access This chapter is licensed under the terms of the Creative Commons Attribution-NonCommercial-NoDerivatives 4.0 International License (http://creativecommons.org/licenses/by-nc-nd/4.0/), which permits any noncommercial use, sharing, distribution and reproduction in any medium or format, as long as you give appropriate credit to the original author(s) and the source, provide a link to the Creative Commons license and indicate if you modified the licensed material. You do not have permission under this license to share adapted material derived from this chapter or parts of it.

The images or other third party material in this chapter are included in the chapter's Creative Commons license, unless indicated otherwise in a credit line to the material. If material is not included in the chapter's Creative Commons license and your intended use is not permitted by statutory regulation or exceeds the permitted use, you will need to obtain permission directly from the copyright holder.

